Numerical simulation of hot smoke plumes from funnels

Ahmad FAKHARI [b], Carlo CINTOLESI [a], Andrea PETRONIO [a], Federico ROMAN [a,1], and Vincenzo ARMENIO [b]

[a] *Iefluids s.r.l., Trieste, Italy*
[b] *Università degli Studi di Trieste*

Abstract. The flow around ship over-structures is characterized by both separation phenomena with recirculation regions at high Reynolds number, and the fast ejection of hot smokes from chimneys. These two features are of the utmost importance for two linked goals in the ship design, namely the aerodynamic drag reduction and the preservations of passengers comfort. In particular, the latter depends on different flow aspects, among the others: the turbulent fluctuations intensity, the smoke temperature and pollutant dispersion and the flow induced noise. In this work, we present an open-source solver developed in OpenFOAM® that is especially suited for the analysis of ship over-structures. It adopts Large-eddy simulation approach and implements an in-house version of the dynamic Lagrangian Sub-grid Scale LES model along with an equilibrium stress wall function in order to deal with high Reynolds number simulations. Furthermore, a synthetic turbulent inflow generation has been developed to provide a more realistic condition. The hot smoke plumes are reproduced considering the buoyancy effect through the Boussinesq approximations. The model has been validated on different benchmark cases and an analysis of a real ship over-structure is presented.

Keywords. ship over-structures, large eddy simulation, buoyant plume, pollution

1. Introduction

In the present study we tackle the problem of the flow over the superstructure of ship, and we propose a numerical model useful in its design. The flow over a superstructure is characterized by a high Reynolds number, in the order of 10^7, which exhibits massive separation regions, both originated from geometrical discontinuities, i.e. sharp edges, or adverse pressure gradients along curved surfaces, as for example the hull. These regions are important from the design point of view because they rule the aerodynamic drag and the passengers comfort. The latter can be affected by the dispersion of smokes, odours and pollutants from chimney

[1]Corresponding Author: Federico Roman, Iefluids s.r.l., Piazzale Europa 1, 34127, Trieste, Italy; E-mail: f.roman@iefluids.com.

stacks, and by the generation of aero-acoustic noise. Moreover, the correct prediction of the flow characteristics in these regions can give useful insights about thermal comfort which is highly sensitive respect to turbulence fluctuations. Such goals can be achieved by means of high-definition unsteady simulation based on Large Eddies Simulation (LES), which are becoming affordable and also necessary in industrial application such as the ship superstructure design. In this study a state-of-art numerical model is implemented in the open-source OpenFOAM® environment, introduced in 2. The density variation caused by temperature gradients, gives rise to buoyancy effects that cannot be excluded a-priori in simulating hot smoke ejection from the ship funnels. The buoyancy force is considered in the model through the Boussinesq approximation. The model solves the filtered Navier-Stokes equations in which the large and energy-carrying structures are directly computed, while the subgrid-scale model parametrizes the small and dissipative turbulent eddies. In-house version of the dynamic Lagrangian Subgrid Scale LES model, which is particularly suited for tackling flows over complex geometry, is implemented. Some details are given in 2.1. In order to reduce the computational effort of such simulation, we implement a reliable wall function, which is described in 2.2. Finally, in order to provide a turbulent inlet profile with coherent fluctuation of velocities, as required for a LES simulation, we implement, as described in 2.3, the synthetic turbulent inflow generation method proposed in [1].

The paper is organized as follows: in section 2 the mathematical models are briefly introduced, then in section 3 benchmark cases for validation sake are discussed for the the turbulence and wall function (3.1) without buoyancy and with buoyancy (3.3), and for the synthetic turbulent inflow method (3.2). In section 4 the case of hot smoke plumes from a ship's funnels is analysed. Finally we draw some conclusions in section 5.

2. Mathematical model

The incompressible formulation of Navier-Stokes equations are considered along with the Boussinesq approximation accounting for the temperature as an active scalar, which triggers buoyancy:

$$\frac{\partial u_i}{\partial x_i} = 0, \tag{1}$$

$$\frac{\partial u_i}{\partial t} + u_k \frac{\partial u_i}{\partial x_k} = -\frac{1}{\rho_0}\frac{\partial p}{\partial x_i} + \nu \frac{\partial^2 u_i}{\partial x_k \partial x_k} - \frac{\rho}{\rho_0} g \delta_{iz}, \tag{2}$$

$$\frac{\rho}{\rho_0} = 1 - \beta_T \Delta T, \tag{3}$$

$$\frac{\partial T}{\partial t} + u_i \frac{\partial T}{\partial x_i} = \alpha \frac{\partial^2 T}{\partial x_i \partial x_i}, \tag{4}$$

where ρ_0, g, β_T, ΔT, α, are the reference density, gravity acceleration, thermal expansion coefficient, temperature variation and the temperature diffusivity respectively.

2.1. Turbulence model

LES with a dynamic Lagrangian Smagorisnky sub-grid scale (SGS) model as proposed by [2] is implemented. Considering the length scale $l \sim \overline{\Delta}$, the eddy viscosity can be writtes as:

$$\nu_{SGS} = (C_s\overline{\Delta})^2 \left|\overline{S}\right|, \tag{5}$$

in which $\overline{\Delta}$ is the filter width, $\left|\overline{S}\right| = \sqrt{2\overline{S}_{ij}\overline{S}_{ij}}$ is contraction of strain rate tensor of the large scales, $\overline{S}_{ij}$. The dynamic computation of the constant based on averaging along fluid trajectories, correctly damps the values of ν_{SGS} close to curved surfaces. The implementation of the model is based on the conclusion of [2], in which the Smagorinsky constant C_s is given by:

$$C_s^2(x,t) = \frac{\mathcal{F}_{LM}}{\mathcal{F}_{MM}} \tag{6}$$

where the values of $\mathcal{F}_{LM}$ and $\mathcal{F}_{MM}$ are solution of the associated differential equation given by

$$\mathcal{F}_{LM}^{n+1}(x) = H\{\epsilon\left[L_{ij}M_{ij}\right]^{n+1}(x) + (1-\epsilon)\,\mathcal{F}_{LM}^{n}\left(x - \overline{u}^n\Delta t\right)\} \tag{7}$$

$$\mathcal{F}_{MM}^{n+1}(x) = \epsilon\left[M_{ij}M_{ij}\right]^{n+1}(x) + (1-\epsilon)\,\mathcal{F}_{MM}^{n}\left(x - \overline{u}^n\Delta t\right) \tag{8}$$

with

$$M_{ij} = 2\Delta^2\left[\left|\overline{S}\right|\overline{S}_{ij} - 4\left|\widehat{\overline{S}}\right|\widehat{\overline{S}}_{ij}\right],\ \epsilon = \frac{\Delta t/T^n}{1+\Delta t/T^n},\ T^n = 1.5\Delta\left(\mathcal{F}_{LM}^n\mathcal{F}_{MM}^n\right)^{-1/8} \tag{9}$$

and $H\{x\}$ is the ramp function. Respect to the available OpenFoam implementation, the simulation is computationally cheaper, and the solution is found to be more stable and robust. In a similar manner, the same filtering and modelling procedure is applied to the active scalar equation (4) accounting for SGS flux $\lambda_i = \overline{Tu_i} - \overline{T}\ \overline{u}_i$. The dynamic Lagrangian approach closes the equation, more details on this can be found in [3], [4].

2.2. Wall-layer model

An equilibrium wall stress model is implemented in which the wall stress is obtained from instantaneous horizontal velocity at the first off-wall centroid based on law of the wall:

$$u_p^+ = \begin{cases} \frac{1}{\kappa}ln\left(y_p^+\right) + B & if \quad y_p^+ > 11 \\ y_p^+ & if \quad y_p^+ \leq 11 \end{cases} \tag{10}$$

where $u_p^+ = u_p/u_\tau = \sqrt{u^2+w^2}/u_\tau$ is the modulus of instantaneous non dimensional velocity at the first off-wall computational node P, which has a distance y_p from the wall, with $\kappa = 0.41$ is the von Kármán constant and $B = 5.1$. The

friction velocity u_τ is calculated from the velocity u_p at each P point base on the linear or logarithmic law, depending on the distance from the wall y_p^+. Then wall shear stress τ_w is obtained as $\tau_w = \rho u_\tau^2$.

Moreover, since the numerical evaluation of the leading terms of $\overline{S}_{ij}$ in the computation of ν_{SGS}, becomes increasingly wrong with decreasing grid resolution, they are replaced by the analytical values based on the location of y_p:

$$\begin{cases} \overline{S}_{12} = \dfrac{u_\tau}{\kappa y_p}\dfrac{\overline{u}}{u_p} + \dfrac{\partial \overline{v}}{\partial x}\ , \quad \overline{S}_{32} = \dfrac{u_\tau}{\kappa y_p}\dfrac{\overline{w}}{u_p} + \dfrac{\partial \overline{v}}{\partial z} & if \quad y_p^+ > 11 \\ \overline{S}_{12} = \dfrac{u_\tau^2}{\nu}\dfrac{\overline{u}}{u_p} + \dfrac{\partial \overline{v}}{\partial x}\ , \quad \overline{S}_{32} = \dfrac{u_\tau^2}{\nu}\dfrac{\overline{w}}{u_p} + \dfrac{\partial \overline{v}}{\partial z} & if \quad y_p^+ \leq 11 \end{cases} \tag{11}$$

Consequently the value of eddy viscosity near the wall adjusts consistently with the imposed stress.

2.3. Turbulent inflow generation

A turbulence generation method is implemented following the procedure proposed in [1]. In the buffer region ad-hoc body-force b' is computed to trigger turbulence properly taking advantage only of average inlet profiles of velocity, U_{RANS}, and turbulent kinetic energy, TKE_{RANS}. The method is based on a simplified TKE transport equation. At the first time step, the fluctuations are absent, the transport equation for TKE and b' are computed:

$$\frac{\partial TKE}{\partial t} =< b_i' u_i' >, \qquad b_i' = \frac{TKE_{RANS}}{u_i' \Delta t}, \qquad u_i' = c_i U_{RANS_i} R \tag{12}$$

with u_i' the fluctuation velocity. A zero mean random number R is multiplied by the reference velocity in order to generate velocity fluctuations at the first time step, with c_i a coefficient bigger than one in order to add some percentages of the mean velocity as fluctuations. Body force is added to right hand side of the momentum equation. The computed b' is multiplied by a ramp function set to be one at the inlet and zero at the end of the buffer region.

3. Validation over benchmark cases

3.1. Plane channel flow

The turbulence model along with the wall function described in 2.1 and 2.2 are tested on the plane channel flow at Reynolds number based on shear velocity $Re_\tau = 4200$. The computational domain has size of $6.25\delta \times \delta \times 3.125\delta$, with resolution of $100 \times 32 \times 50$ uniform cells in stream-wise (x), wall-normal (y) and span-wise (z) directions respectively.

Periodic boundary conditions are enforced in stream and span-wise directions, while wall function is applied on upper and lower walls. The flow is driven by an uniform pressure gradient as a body-force in x direction. For testing purposes

a standard Smagorinsky is firstly applied showing that the mean-velocity and the root mean square of its fluctuations provided the best results for maximum Courant number of $Co = 0.1$ respect larger values of Co. The rms of the velocity fluctuations were slightly underestimated near the centre of the channel compared to DNS by Hoyas and Jiménez [5].

A comparison of the performance of the implemented wall function with the `nuSgsUSpaldingWallFunction` available in OpenFoam, from now on referred as OF wall function is carried out on a grid with resolution of $100 \times 50 \times 50$ cells. The results reveal that the OF wall function overpredicts the mean velocity profile everywhere except at the first computational node (figure 1a). Meanwhile, figure 1b shows that the OF wall function underrates the rms of velocity fluctuations close to the wall. In general the equilibrium wall stress wall function provides more accurate results both in terms of averaged velocity profile and of rms fluctuations.

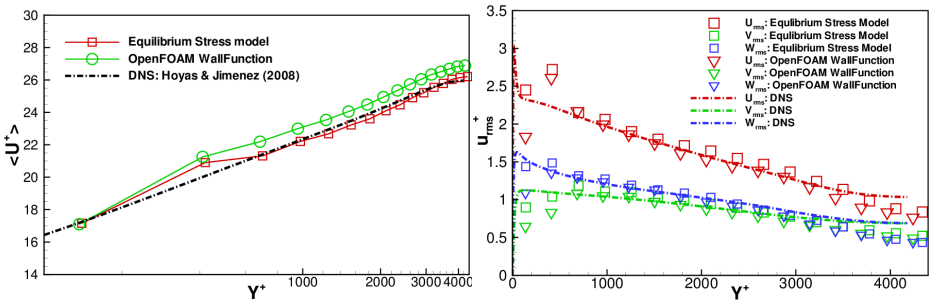

(a) Mean velocity profile. (b) rms of velocity fluctuations.

Figure 1. Mean velocity and rms of the velocity fluctuations using equilibrium stress wall function versus wall function in OF for the case with 32 cells in span-wise direction;

3.2. Validation of turbulent inflow

The turbulent inflow boundary condition introduced in 2.3, is tested along with the dynamic Lagrangian SGS model on a plane channel flow at $Re_\tau = 1000$ driven by unit value of pressure gradient as body-force in stream-wise direction with a domain size of $2\pi\delta \times 2\delta \times \pi\delta$ with the resolution of $48 \times 32 \times 32$ cells in stream-wise, wall normal and span-wise directions respectively. The mean stream-wise velocity and rms of the velocity fluctuations have been calculated and plotted at the middle of buffer region ($x = 0.5\delta$), at the buffer edge ($x = \delta$) and five other sections in stream-wise directions with a distance of δ between consecutive sections.

The simulation is carried out at $Co = 0.1$, and considering a buffer length of δ spanning over 8 cells in stream-wise direction. Figure 2 shows velocity profiles at seven different stream-wise locations and the quantities are non-dimentionalized using theoretical shear velocity ($u_\tau = 1\ m/s$). The mean velocity profiles in figure 2a shows that the mean velocity near wall inside the buffer region is underval-

ued, while outside this region near wall velocity decreases slightly in stream-wise direction and there is a marginal undervaluation at the end of the channel. Also the rms predictions are in good agreement with respect to the expected results and compared with DNS data.

For example in figure 2b is shown that rms of wall normal fluctuations inside and outside of the buffer region going farther from wall, are a bit underrated, but in general a good agreement is achieved with DNS profile.

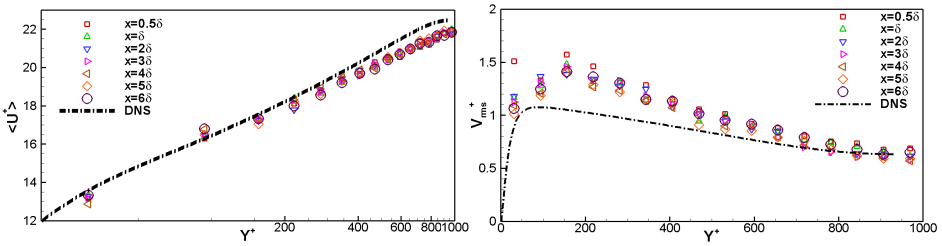

(a) Mean velocity profile.

(b) rms of wall normal velocity fluctuations.

Figure 2. Mean velocity and rms of the velocity fluctuations using our turbulent inflow boundary condition and equilibrium stress wall function and dynamic Lagrangian SGS model at $Re_\tau = 1000$ compare to DNS by Hoyas and Jiménez [5] at $Re_\tau = 936$.

3.3. Buoyant jet in cross flow

For validation purposes, here is reproduced the experiment studied in [6], called Run 10-8, about a round buoyant jet in uniform cross-flow. The case sketch is reported in figure 3a. An extensive study on the subject is presented in [7]. The non-dimensional parameters ruling such flow are the Froude number F, velocity ratio κ, and Reynolds number Re, defined as follows

$$F = \frac{u_{j0}}{\sqrt{\beta_T \Delta T\, gD}} = 10, \qquad Re = \frac{u_{j0} D}{\nu} = 8\,200, \qquad \kappa = \frac{u_{j0}}{u_{cf}} = 8, \tag{13}$$

where u_{j0}, u_{cf}, D are the jet and cross flow velocities, and the jet nozzle diameter respectively; ΔT is the difference between the environment value and the hot air from the nozzle. The boundary conditions are a constant velocity u_{cf} in x-direction and temperature of $T_{cf} = 0$ at the inlet; a constant velocity u_{cf} in x-direction and zero-gradient for temperature at lateral and top boundaries; no-slip condition for velocity and zero-gradient for temperature at bottom and nozzle cylinder boundaries; at nozzle exit is imposed a constant velocity u_{j0} in z-direction and a fixed temperature; zero-gradient condition is applied for both for the scalar and velocity at the outlet. Pressure is fixed as $p = 0$ at the outlet, while the zero-gradient condition is set elsewhere.

The instantaneous plume is plotted on the experimental picture of the smoke for a qualitative comparison in figure 3b. The LES plume, visualised by $T = 0.01$ isosurface, overlaps to the experimental plume isosurface. Overall, a good agreement is found. More results on this case are reported in [7].

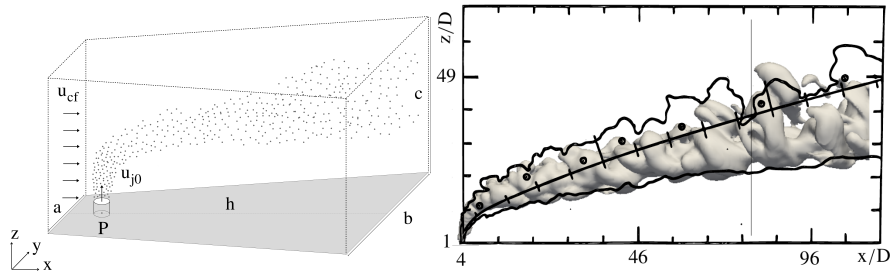

(a) Geometry sketch.

(b) Result comparison: overlap of experimental plume profile with simulated one.

Figure 3. Sketch of the geometry of the experiment (nozzle is not in scale) (a) and qualitative comparison between experiment [6] and LES plume (visualised by $T = 0.01\Delta T$ isosurface) (b).

4. Application to the hot smoke plume from ship's funnels

The numerical model is finally applied on the over structure of a ship, with three funnels ejecting hot smokes. A contour plot of instantaneous velocity field is shown in figure 4a, along a vertical section on the middle of the ship. The ship geometry is hidden by blue squares for sake of confidentiality. In front of the ship, the inflow section provides an uniform reference temperature and an averaged atmospherical boundary layer profiles of velocity and TKE, in order to correctly feed the turbulent buffer. Some of the artificially generated fluctuations are visible in the first cell layers close to the inflow. At the outlet outflow conditions are enforced. The domain bottom is treated as a solid surface, while slip conditions are applied on lateral and top boundaries. In figure 4a the region behind the funnels from the top of the ship is magnified. The dark black streak in the contour plot represents the fast hot smoke ejected from the funnel. The grey and light grey in the contour plot in the rear of the funnel shows the recirculation region and the wake of the ship.

5. Conclusions

We presented a state-of-art numerical tool for simulation of flow over ship's superstructures. It implements the dynamic Lagrangian SGS LES model to cope with complex geometry and the Boussinesq approximation for the buoyancy arising from hot smokes from funnels' ship. The equilibrium stress wall model permits to reduce the number of computational cells required to correctly reproduce the flow close to solid surfaces. Moreover a synthetic turbulence inflow generation method is included allowing the generation of proper velocity fluctuation at the entrance of the domain. All the modules are tested on benchmark cases, and the correct reproduction of a buoyant jet in a cross flow is shown, as an archetypical case of the smoke from ship's chimneys. Finally, a simulation of a ship with three funnels is briefly presented. In general the model performs good in all the benchmark cases, and the ship application shows realistic results.

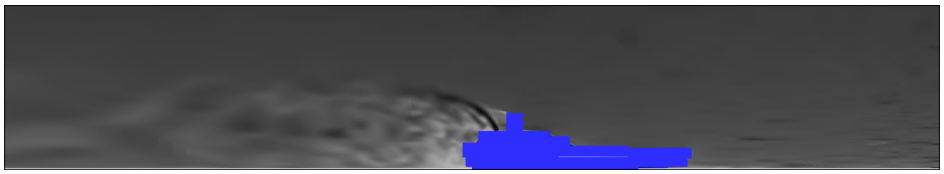

(a) Instantaneous velocity contour.

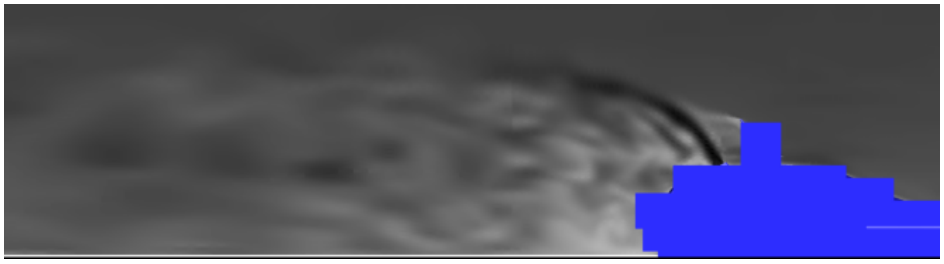

(b) Instantaneous velocity contour, details in the recirculation region behind the funnels.

Figure 4. Instantaneous velocity contour on a vertical section, the velocity magnitude contour range from white, zero velocity, to black, for highest velocity in the domain.

Aknowledgement

This work was supported by Region FVG-PAR FSC 2007–2013, Fondo per lo Sviluppo e la Coesione, Project COSMO CFD open source per opera morta".

References

[1] A. Petronio, F. Roman, C. Nasello and V. Armenio, Large-Eddy Simulation model for wind driven sea circulation in coastal areas, *Nonlinear Processes in Geophysics* **20** (2013), 1095–1112.

[2] C. Meneveau, T.S. Lund, W. H. Cabot, A Lagrangian dynamic subgrid-scale model of turbulence, *Journal of Fluid Mechanics* **319** (1996), 353–385.

[3] C. Cintolesi, A. Petronio, V. Armenio, Large-eddy simulation of thin film evaporation and condensation from a hot plate in enclosure: first order statistics, *International Journal of Heat and Mass Transfer* **101** (2016) 1123.

[4] C. Cintolesi, A. Petronio, and Vincenzo Armenio, Large-eddy simulation of thin film evaporation and condensation from a hot plate in enclosure: Second order statistics, *International Journal of Heat and Mass Transfer* **115** (2017) 410–423.

[5] Hoyas, S. and Jimenez, J. (2008), Reynolds number effects on the Reynolds-stress budgets in turbulent channels, *J. Phys. Fluids*, **20**, 101511, 1–8.

[6] L.N. Fan, Turbulent buoyant jets into stratified or flowing ambient fluids, *Ph.D.thesis*, California Institute of Technology, (1967).

[7] C. Cintolesi, A. Petronio, V. Armenio, Turbulent structures of buoyant jet in cross-flow studied through large-eddy simulation, *Environmental Fluid Mechanics, submitted*

[8] C. Cintolesi, A. Petronio, V. Armenio, Large eddy simulation of turbulent buoyant flow in a confined cavity with conjugate heat transfer, *Physics of Fluids***27** (2015).

[9] Cabot W., Moin P. (2000): Approximate wall boundary conditions in the large-eddy simulation of high Reynolds number flows, *Flow. Turbul. Combust.* , **63**, 269–291